Magnetotelluric evidence for thick-skinned tectonics in central Taiwan

Edward Bertrand[1], Martyn Unsworth[1], Chih-Wen Chiang[2], Chow-Son Chen[2], Chien-Chih Chen[2], Francis Wu[3], Erşan Türkoğlu[1], Han-Lun Hsu[2], and Graham Hill[4]

[1]Department of Physics, University of Alberta, Edmonton, Alberta T6G 2R3, Canada
[2]Institute of Geophysics, National Central University, Chung-Li, Taiwan
[3]State University of New York at Binghamton, Binghamton, New York 13902-6000, USA
[4]Institute of Geological and Nuclear Sciences, Lower Hutt 5010, New Zealand

ABSTRACT

Taiwan is the type example of an arc-continent collision. Numerous tectonic models have been proposed for this orogen, and include both thin-skinned and thick-skinned lithospheric deformation. These models predict very different structures at middle and lower crustal depths, but insufficient geophysical data exist to unequivocally distinguish between them. Long-period magnetotelluric (MT) data were collected in central Taiwan in 2006–2007 to constrain the crustal resistivity structure. A two-dimensional inversion of these MT data revealed a prominent electrical conductor that extends across the décollement predicted by the thin-skinned model. This feature is interpreted to be due to 1%–2% saline fluids, and is inconsistent with the thin-skinned model. In contrast, the thick-skinned model predicts this feature since fluids are generated in the crustal root through metamorphism. Quantitative correlation of the resistivity and seismic velocity models supports small-volume, high-salinity fluids in a thickened crust as the cause of this conductor.

INTRODUCTION

Arc-continent collisions are a fundamental tectonic process and contribute to continental growth. In ancient collisions, postorogenic geological events obscure the orogenic processes, thus studies of active collisions are needed. The oblique convergence between the Luzon Volcanic Arc and the passive margin of the Eurasian plate represents the best example of an active arc-continent collision. Since the late Miocene, convergence has produced a mature orogen in northern Taiwan, the collision becoming younger to the south (Byrne and Liu, 2002). Several models have been proposed to explain the collision tectonics of central Taiwan, and these models form a spectrum between two end members: (1) thin-skinned tectonics, and (2) thick-skinned lithospheric deformation.

In the thin-skinned model, a shallow décollement dips east within the upper continental crust. Deformation is localized above this surface while the Eurasian continental lithosphere subducts below. The thin-skinned model was motivated by geological and shallow seismic exploration in the Western Foothills fold-and-thrust belt (Suppe, 1981). Near-surface deformation in the Western Foothills (Yue et al., 2005) and surface heat flow (Bahr and Dahlen, 1990) are consistent with predictions from critical wedge theory employing a shallow décollement. In addition, earthquake hypocenters have been moved under certain assumptions to infer that a band of seismicity exists at 8–10 km depth from the Western Foothills to the Coastal Range, which is interpreted to be the décollement (Carena et al., 2002).

In contrast, the thick-skinned model predicts continuous deformation throughout the lithosphere, with prograde metamorphism occurring within a thickened crust beneath the Central Ranges (Wu et al., 1997). This model is supported by observation of a crustal root in seismic tomography models (Wu et al., 2007) and by precisely relocated hypocenters (Wu et al., 2004). Receiver function analysis (Kim et al., 2004), TAICRUST active source seismic data (McIntosh et al., 2005), shear wave splitting (Rau et al., 2000), and gravity data (Yen et al., 1998) also support the thick-skinned model.

Existing geophysical data could not distinguish between these end-member models beneath the Central Ranges, thus additional data were needed. As part of the Taiwan Integrated Geodynamics Research (TAIGER) project, the first long-period (10–10000 s) MT data were collected in Taiwan. MT measurements image subsurface electrical resistivity and can provide constraints on lithospheric composition and strength (Unsworth et al., 2005). This paper describes the collection and interpretation of the TAIGER MT data in central Taiwan.

MAGNETOTELLURIC DATA COLLECTION AND ANALYSIS

MT measurements use natural electromagnetic (EM) fields to image subsurface resistivity structure. The penetration depth of these signals increases with period (Simpson and Bahr, 2005). In 2006–2007, long-period MT data were recorded at 21 stations in central Taiwan and at a remote reference station on the Penghu archipelago to reduce cultural EM noise (Fig. 1). The study area is located in a region of complex geology and

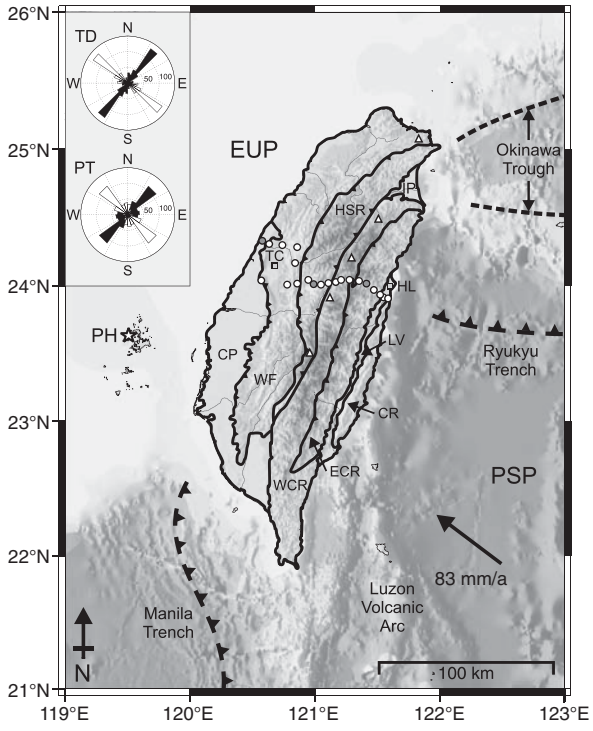

Figure 1. Regional geologic and tectonic map of Taiwan. White circles denote long-period magnetotelluric stations; gray circles indicate where only magnetic field data were analyzed; white triangles show locations of Au-Cu deposits. Star marks remote reference station on Penghu (PH) archipelago. EUP—Eurasian plate; PSP—Philippine Sea plate. Geological provinces: CP—Coastal Plain; WF—Western Foothills; HSR—Hseuhshan Range; WCR—West Central Range; ECR—East Central Range; LV—Longitudinal Valley; CR—Coastal Range; IP—Ilan Plain. Cities: TC—Taichung; HL—Hualien. Rose diagrams show geoelectric strike direction computed from tensor decomposition (TD) and phase tensor (PT) analysis for periods 10–3000 s. Black and white sectors are equivalent, as there is inherent 90° ambiguity in strike direction determined by these methods.

is surrounded by ocean with variable water depths. These factors require careful data analysis to determine if a two-dimensional (2-D) or three-dimensional (3-D) interpretation is appropriate. The dimensionality and geoelectric strike direction were investigated using both tensor decomposition (McNeice and Jones, 2001) and phase tensor analysis (Caldwell et al., 2004). These techniques found a consistent strike direction (N37°E) that is parallel to the major geological boundaries (Fig. 1; Fig. DR1 in the GSA Data Repository[1]). Induction vectors can also determine the dimensionality (Simpson and Bahr, 2005). Within the period band 10–100 s the induction vectors are predominantly perpendicular to the geoelectric strike, indicating 2-D conductivity structure (Fig. DR2). EM signals at these periods are sensitive to mid-crustal depths, where major differences are predicted between the end-member models. At periods >1000 s, the induction vectors point east due to the large conductance of the Philippine Sea. For periods 100–1000 s, induction vectors in eastern Taiwan mainly point northeast, indicating 3-D conductivity structure. Despite this 3-D evidence, the well-defined strike direction and the 2-D nature of the induction vectors at periods most sensitive to the upper and middle crust justify a 2-D analysis. The 2-D inversion algorithm of Rodi and Mackie (2001) was used to generate smooth resistivity models. An inversion of the MT impedances and induction vector data produced a model that fits the observations (Fig. 2A). MT data showing high levels of distortion and/or noise were excluded to allow a good fit by the inversion (root mean square misfit = 1.3; Figs. DR3 and DR4).

INTERPRETATION

Resistivity Model

Conductive (low resistivity) sedimentary rocks are imaged in the foreland basin of western Taiwan (FBC in Fig. 2A). East of this zone, resistivity increases where the sedimentary rocks contact the metamorphic rocks of the Hseuhshan Range. While limited in near-surface resolution, this model does not support underthrusting of the conductive Western Foothills rocks beneath the Hseuhshan Range. The steep contact imaged between these provinces favors the thick-skinned tectonic model. The boundary between the Hseuhshan Range and West Central Range coincides with the west-dipping Lishan fault, suggested to border the eastern edge of an Oligocene half-graben (Clark et al., 1993).

In eastern Taiwan, a near-surface conductor (LVC in Fig. 2A) that may be related to fluids coincides with the Longitudinal Valley fault (Yu and Kuo, 2001, their figure 2). This active, high-angle oblique thrust fault overlies the suture zone between the Eurasian plate and the Philippine Sea plate (Yu and Kuo, 2001). However, this model feature is poorly resolved, owing to its location near the end of the profile and the insensitivity of long-period MT data to near surface structure.

A prominent feature of the resistivity model is the mid-crustal conductor (LFC in Fig. 2A) located beneath the Lishan fault. Partial melts and/or aqueous fluids have been proposed to explain similar crustal conductors elsewhere (Wannamaker et al., 2002; Unsworth et al., 2005).

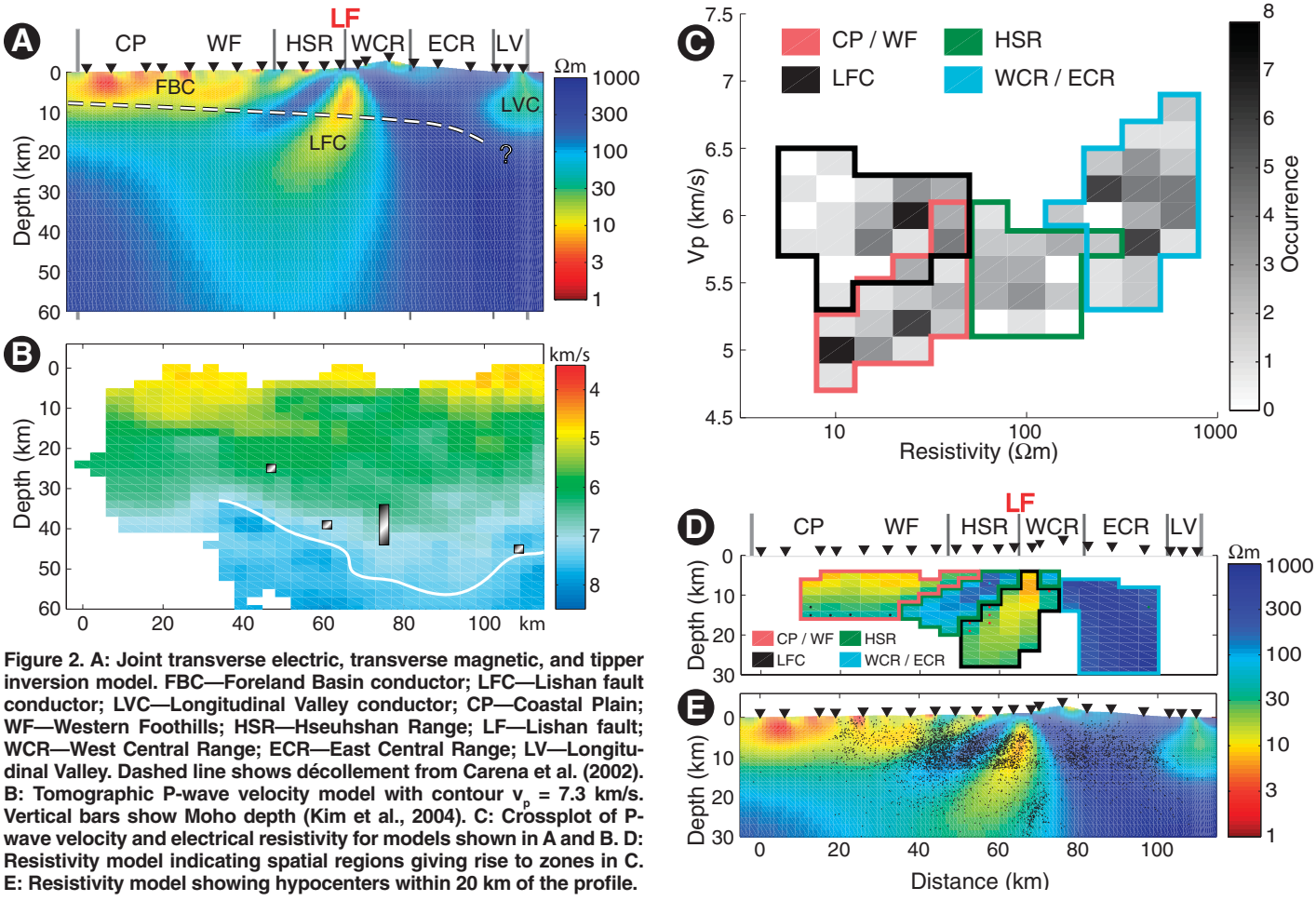

Figure 2. A: Joint transverse electric, transverse magnetic, and tipper inversion model. FBC—Foreland Basin conductor; LFC—Lishan fault conductor; LVC—Longitudinal Valley conductor; CP—Coastal Plain; WF—Western Foothills; HSR—Hseuhshan Range; LF—Lishan fault; WCR—West Central Range; ECR—East Central Range; LV—Longitudinal Valley. Dashed line shows décollement from Carena et al. (2002). B: Tomographic P-wave velocity model with contour v_p = 7.3 km/s. Vertical bars show Moho depth (Kim et al., 2004). C: Crossplot of P-wave velocity and electrical resistivity for models shown in A and B. D: Resistivity model indicating spatial regions giving rise to zones in C. E: Resistivity model showing hypocenters within 20 km of the profile.

[1]GSA Data Repository item 2009171, supplemental information and figures, is available online at www.geosociety.org/pubs/ft2009.htm, or on request from editing@geosociety.org or Documents Secretary, GSA, P.O. Box 9140, Boulder, CO 80301, USA.

Given the relatively shallow depth and thermal conditions of the Lishan fault, a distributed zone of saline fluids in the middle to lower crust is the most likely cause of the low resistivity.

The Lishan fault conductor appears to cross the location of the décollement proposed by Carena et al. (2002). If the Lishan fault conductor is caused by a zone of interconnected aqueous fluids, then this is significant in terms of the depth extent of deformation in central Taiwan. The presence of such a feature is consistent with a thick-skinned model since interconnected fluids would be released below 10–15 km depth as the crust is thickened. A feature similar to the Lishan fault conductor was observed in an MT study of the South Island of New Zealand (Wannamaker et al., 2002) and was attributed to fluids released from prograde metamorphism within a thickened crust. The presence of the Lishan fault conductor presents two challenges to the thin-skinned model. First, with minimal deformation below the décollement, it is difficult to envision a mechanism to generate fluids at shallow depths within the subducting Eurasian plate. Second, if a décollement were present, it might be expected to disrupt upward fluid migration.

Identifying whether the Lishan fault conductor extends into the mid-crust has significant tectonic implications. However, resolving the depth extent presents a challenge, since MT data are primarily sensitive to the depth to the top of a conductor. Smooth inversions often smear conductive features to depth, thus a series of constrained inversions were implemented with models fixed to be resistive below a given depth. The fit to the observed tipper data (ratio of vertical to horizontal magnetic fields) adjacent to the Lishan fault is illustrated in Figure 3. Note that these inversions also fit the MT impedances; however, only the tipper responses are shown as these data are most sensitive to vertical structure (Unsworth et al., 2000). Progressively decreasing the depth to the resistive basement causes an increase in the data misfit; the depth at which this occurs corresponds to the shallowest conductor permitted by the data (Li et al., 2003). The F30 model fits the measured data very well (Fig. 3). The misfit is higher in the F20 model, but is still acceptable. In contrast, the F10 model does not adequately fit the measured data, indicating that the Lishan fault conductor extends beyond a depth of 10 km. Conductance plots of these constrained inversions also indicate a poor fit to the F10 model (Figs. DR5 and DR6).

The presence of a conductive feature extending across the depth of the inferred décollement is difficult to reconcile with a thin-skinned model and is interpreted as support for the thick-skinned lithospheric deformation model of Wu et al. (1997).

Correlation of Resistivity and Seismic Velocity

Integration of independent geophysical data was implemented by comparing a seismic velocity model and relocated earthquake hypocenters with the resistivity model. The tomographic model consists of P-wave velocity estimates on an x = y = 5, z = 2 km grid, and incorporates first-arrival data from TAIGER active seismic transects in 2007–2008. Hypocenter locations for M > 2 events from 1993 to 2002 were obtained using the double-difference relocation method (Wu et al., 2004).

The resistivity and velocity models (Figs. 2A and 2B) are clearly correlated. For example, both models have their lowest values in the upper 10 km beneath the Coastal Plain and Western Foothills. However, a quantitative approach is required to determine the degree to which these parameters are related. The method of Bedrosian et al. (2004) was used to determine distinct model domains that are defined by ranges of velocity and resistivity. The resistivity model was first interpolated onto the same grid as the velocity model, and poorly resolved areas of the models were masked to avoid correlation of unconstrained parameter estimates. For example, conductors are smeared to depth by the regularized inversion, thus cells beneath large conductors were excluded from the analysis. Model edges were also masked where features are poorly resolved. A histogram of the occurrence of resistivity and velocity combinations for each model cell was then generated (Fig. 2C). Distinct domains within this histogram are identified and mapped back onto the resistivity model (Fig. 2D).

No universal relationship between resistivity and velocity has been reported for crustal-scale studies (Bedrosian et al., 2007). In general, porosity provides a link between electrical resistivity and seismic velocity (Hacikoylu et al., 2006), since as porosity decreases, both resistivity and velocity increase. Metamorphic grade increases eastward across Taiwan, thus an associated increase in electrical resistivity and seismic velocity is expected. Four distinct domains are observed in the histogram, and three of these (Coastal Plain/Western Foothills, Hseuhshan Range, and West Central Range/East Central Range) define a trend of increasing velocity and resistivity with metamorphic grade. However, the Lishan fault conductor domain is not on this trend.

The Lishan fault conductor domain is characterized by an area of anomalously low resistivity and only moderately low velocity. Fluids generated by prograde metamorphism within a thickened crust are the most likely explanation for this conductor. Evidence for extensive fluid circulation in this area comes from a number of sulfide deposits adjacent to the Lishan fault (Fig. 1). Tectonically driven hydrothermal fluid circulation is often associated with mesothermal gold mineralization in young or active orogens (Craw et al., 2002, their table 1). Thus, it is necessary to show that fluids can account for the low resistivities in this domain, without causing a decrease in velocity. At the pressure-temperature conditions present in the middle to lower crust, saline fluid is expected to have a resistivity of ρ_w ~0.01–0.05 Ωm (Nesbitt, 1993). Assuming a cementation factor of m = 1.5, Archie's law (Archie, 1942) requires porosity values of 1%–2% to explain a bulk resistivity of 15 Ωm. This result is not critically dependent on the values of the parameters used in Archie's Law (Fig. DR7). Laboratory measurements indicate little change in P-wave velocity with varying pore-fluid salinity (Jones et al., 1998). Thus, a porosity of a few percent saturated with saline fluid is consistent with both the velocity and resistivity constraints on the Lishan fault conductor.

Correlation of Resistivity and Hypocenter Locations

Links between resistivity and seismicity have been noted in previous studies (Chen et al., 2007; Ogawa et al., 2001). Of interest in central Taiwan is a cluster of deep (20–30 km) seismicity located near the eastern edge of the Lishan fault conductor (Fig. 2E). Focal mechanisms suggest that these epicenters are associated with a thrust fault, with the Central Ranges on the footwall side (Wu et al., 2004). Gourley et al. (2007) recognized this and other evidence for deep vertical faults within the Central Ranges that would contribute to building a crustal root. The location adjacent to the Lishan fault conductor suggests that this fault may act as a conduit for fluid migration toward the surface.

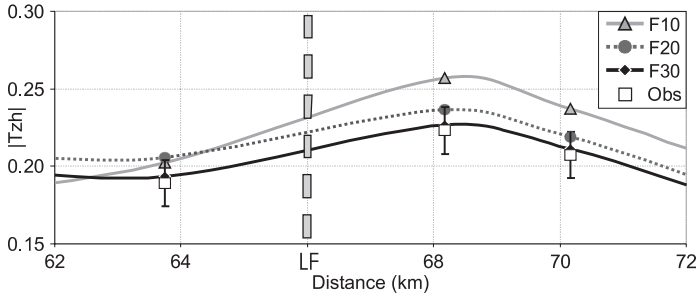

Figure 3. Tipper data projected parallel to profile at period of 100 s for stations adjacent to the Lishan fault (LF). Open squares (Obs) denote measured data with absolute error floor of 0.03. Smooth curves are responses of constrained inversion models with resistive (300 Ωm) basement fixed at depths 10, 20, and 30 km (models F10, F20, and F30, respectively).

CONCLUSIONS

A resistivity model of the first long-period MT data collected in central Taiwan reveals a major conductor located beneath the Lishan fault that extends from the near surface to beyond 10 km depth. The shallow décollement predicted by the thin-skinned tectonic model is consistent with the MT data in western Taiwan, but not with the Lishan fault conductor in central Taiwan. Quantitative correlation between the resistivity and a tomographic velocity model indicates that aqueous fluids with 1%–2% porosity can account for the Lishan fault conductor. The thick-skinned lithospheric deformation model is consistent with these observations, with the fluids being produced in the lower crust by prograde metamorphism.

ACKNOWLEDGMENTS

This research was funded by the National Sciences and Engineering Research Council of Canada, National Science Foundation (Continental Dynamics Program) under award EAR0410227, Alberta Ingenuity Fund, National Central University of Taiwan, and the University of Alberta, Canada. Assistance from landowners in Taiwan is appreciated. We thank Randy Mackie for use of his inversion algorithm, and Alan Jones and Gary McNeice for their tensor decomposition software. Constructive reviews by Phil Wannamaker and David Wiltscko are greatly appreciated.

REFERENCES CITED

Archie, G.E., 1942, The electrical resistivity log as an aid in determining some reservoir characteristics: American Institute of Mining: Metallurgical and Petroleum Engineers Transactions, v. 146, p. 54–62.

Bahr, T.D., and Dahlen, F.A., 1990, Constraints on friction and stress in the Taiwan fold-and-thrust belt from heat flow and geochronology: Geology, v. 18, p. 111–115, doi: 10.1130/0091-7613(1990)018<0111:COFASI>2.3.CO;2.

Bedrosian, P.A., Unsworth, M.J., Egbert, G.D., and Thurber, C.H., 2004, Geophysical images of the creeping segment of the San Andreas fault: Implications for the role of crustal fluids in the earthquake process: Tectonophysics, v. 385, p. 137–158, doi: 10.1016/j.tecto.2004.02.010.

Bedrosian, P.A., Maercklin, N., Weckmann, U., Bartov, Y., Ryberg, T., and Ritter, O., 2007, Lithology-derived structure classification from the joint interpretation of magnetotelluric and seismic models: Geophysical Journal International, v. 170, p. 737–748, doi: 10.1111/j.1365-246X.2007.03440.x.

Byrne, T.B., and Liu, C.S., 2002, Introduction to the geology and geophysics of Taiwan, *in* Byrne, T.B., and Liu, C.S., eds., Geology and geophysics of an arc-continent collision, Taiwan: Geological Society of America Special Paper 358, p. v–viii.

Caldwell, T.G., Bibby, H.M., and Brown, C., 2004, The magnetotelluric phase tensor: Geophysical Journal International, v. 158, p. 457–469, doi: 10.1111/j.1365-246X.2004.02281.x.

Carena, S., Suppe, J., and Kao, H., 2002, Active detachment of Taiwan illuminated by small earthquakes and its control of first-order topography: Geology, v. 30, p. 935–938, doi: 10.1130/0091-7613(2002)030<0935:ADOTIB>2.0.CO;2.

Chen, C.C., Chi, S.C., Chen, C.S., and Yang, C.H., 2007, Electrical structures of the source area of the 1999 Chi-Chi, Taiwan, earthquake: Spatial correlation between crustal conductors and aftershocks: Tectonophysics, v. 443, p. 280–288, doi: 10.1016/j.tecto.2007.01.018.

Clark, M.B., Fisher, D.M., Lu, C.Y., and Chen, C.H., 1993, Kinematic analyses of the Hsuehshan range, Taiwan: A large-scale pop-up structure: Tectonics, v. 12, p. 205–217, doi: 10.1029/92TC01711.

Craw, D., Koons, P.O., Horton, T., and Chamberlain, C.P., 2002, Tectonically driven fluid flow and gold mineralization in active collisional orogenic belts: Comparison between New Zealand and western Himalaya: Tectonophysics, v. 348, p. 135–153, doi: 10.1016/S0040-1951(01)00253-0.

Gourley, J.R., Byrne, T., Chan, Y.C., Wu, F., and Rau, R.J., 2007, Fault geometries illuminated from seismicity in central Taiwan: Implications for crustal scale structural boundaries in the northern Central Range: Tectonophysics, v. 445, p. 168–185, doi: 10.1016/j.tecto.2007.08.013.

Hacikoylu, P., Dvorkin, J., and Mavko, G., 2006, Resistivity-velocity transforms revisited: Leading Edge, v. 25, p. 1006–1009, doi: 10.1190/1.2335159.

Jones, S.M., McCann, C., Astin, T.R., and Sothcott, J., 1998, The effects of pore-fluid salinity on ultrasonic wave propagation in sandstones: Geophysics, v. 63, p. 928–934, doi: 10.1190/1.1444404.

Kim, K.H., Chiu, J.M., Kao, H., Liu, Q., and Yeh, Y.H., 2004, A preliminary study of crustal structure in Taiwan region using receiver function analysis: Geophysical Journal International, v. 159, p. 146–164, doi: 10.1111/j.1365-246X.2004.02344.x.

Li, S., Unsworth, M.J., Booker, J.R., Wei, W., Tan, H., and Jones, A.G., 2003, Partial melt or aqueous fluid in the mid-crust of Southern Tibet? Constraints from INDEPTH magnetotelluric data: Geophysical Journal International, v. 153, p. 289–304, doi: 10.1046/j.1365-246X.2003.01850.x.

McIntosh, K., Nakamura, Y., Wang, T.K., Shih, R.C., Chen, A., and Liu, C.S., 2005, Crustal-scale seismic profiles across Taiwan and the western Philippine Sea: Tectonophysics, v. 401, p. 23–54, doi: 10.1016/j.tecto.2005.02.015.

McNeice, G.W., and Jones, A.G., 2001, Multisite, multifrequency tensor decomposition of magnetotelluric data: Geophysics, v. 66, p. 158–173, doi: 10.1190/1.1444891.

Nesbitt, B., 1993, Electrical resistivities of crustal fluids: Journal of Geophysical Research, v. 98, p. 4301–4310, doi: 10.1029/92JB02576.

Ogawa, Y., Mishina, M., Goto, T., Satoh, H., Oshiman, N., Kasaya, T., Takahashi, Y., Nishitani, T., Sakanaka, S., Uyeshima, M., Takahashi, Y., Honkura, Y., and Matsushima, M., 2001, Magnetotelluric imaging of fluids in intraplate earthquake zones, NE Japan back arc: Geophysical Research Letters, v. 28, p. 3741–3744, doi: 10.1029/2001GL013269.

Rau, R.J., Liang, W.T., Kao, H., and Huang, B.S., 2000, Shear wave anisotropy beneath the Taiwan orogen: Earth and Planetary Science Letters, v. 177, p. 177–192, doi: 10.1016/S0012-821X(00)00058-3.

Rodi, W., and Mackie, R.L., 2001, Nonlinear conjugate gradients algorithm for 2-D magnetotelluric inversion: Geophysics, v. 66, p. 174–187, doi: 10.1190/1.1444893.

Simpson, F., and Bahr, K., 2005, Practical magnetotellurics: Cambridge, Cambridge University Press, 254 p.

Suppe, J., 1981, Mechanics of mountain building and metamorphism in Taiwan: Geological Society of China Memoir, v. 4, p. 67–89.

Unsworth, M., Bedrosian, P., Eisel, M., Egbert, G., and Siripunvaraporn, W., 2000, Along strike variations in the electrical structure of the San Andreas fault at Parkfield, California: Geophysical Research Letters, v. 27, p. 3021–3024, doi: 10.1029/2000GL011476.

Unsworth, M.J., Jones, A.G., Wei, W., Marquis, G., Gokarn, S.G., Spratt, J.E., and the INDEPTH-MT team, 2005, Crustal rheology of the Himalaya and southern Tibet inferred from magnetotelluric data: Nature, v. 438, p. 78–81, doi: 10.1038/nature04154.

Wannamaker, P.E., Jiracek, G.R., Stodt, J.A., Caldwell, T.G., Gonzalez, V.M., McKnight, J.D., and Porter, A.D., 2002, Fluid generation and pathways beneath an active compressional orogen, the New Zealand Southern Alps, inferred from magnetotelluric data: Journal of Geophysical Research, v. 107, 2117, doi: 10.1029/2001JB000186.

Wu, F.T., Rau, R.J., and Slazberg, D., 1997, Taiwan orogeny: Thin-skinned or lithospheric collision?: Tectonophysics, v. 274, p. 191–220, doi: 10.1016/S0040-1951(96)00304-6.

Wu, F.T., Chang, C.S., and Wu, Y.M., 2004, Precisely relocated hypocenters, focal mechanisms and active orogeny in central Taiwan, *in* Malpas, J., et al., eds., Aspects of the tectonic evolution of China: Geological Society of London Special Publication 226, p. 333–354.

Wu, Y.M., Chang, C.H., Zhao, L., Bruce, J., Shyu, H., Chen, Y.G., Sieh, K., and Avouac, J.P., 2007, Seismic tomography of Taiwan: Improved constraints from a dense network of strong motion stations: Journal of Geophysical Research, v. 112, B08312, doi: 10.1029/2007JB004983.

Yen, H.Y., Yeh, Y.H., and Wu, F.T., 1998, Two-dimensional crustal structures of Taiwan from gravity data: Tectonics, v. 17, p. 104–111, doi: 10.1029/97TC02697.

Yu, S.B., and Kuo, L.C., 2001, Present-day crustal motion along the Longitudinal Valley Fault, eastern Taiwan: Tectonophysics, v. 333, p. 199–217, doi: 10.1016/S0040-1951(00)00275-4.

Yue, L.F., Suppe, J., and Hung, J.H., 2005, Structural geology of a classic thrust belt earthquake: The 1999 Chi-Chi earthquake Taiwan (M_w=7.6): Journal of Structural Geology, v. 27, p. 2058–2083, doi: 10.1016/j.jsg.2005.05.020.

Manuscript received 30 December 2008
Revised manuscript received 20 March 2009
Manuscript accepted 24 March 2009

Printed in USA

GSA DATA REPOSITORY 2009171

Supplementary material for "Magnetotelluric evidence for thick-skinned tectonics in central Taiwan".

1. Dimensionality and Distortion of the MT data

Tensor decomposition was used to investigate distortion and to determine the 2-D geoelectric strike direction of the MT data. Results of this analysis are summarized in Figure DR1 and indicate that a good fit was obtained to the measured MT data with only minor galvanic distortion observed at most sites and periods. The vertical magnetic field data can be illustrated by plotting the induction vectors, which provides an independent constraint on dimensionality, because these vectors do not have the same 90° ambiguity as tensor decomposition. The induction vectors are plotted in Figure DR2 and predominately point perpendicular to geological boundaries, indicating an overall 2-Dimensional resistivity structure. These techniques define a geoelectric strike direction of N37°E that is essentially parallel to the geological boundaries.

2. Representative MT data curves

MT data were rotated to the geoelectric strike (N37°E) co-ordinate system and sample MT data curves are plotted in Figure DR3. The transverse electric (TE) mode data is computed from the strike-parallel electric field measurements and strike-perpendicular magnetic fields. Conversely, the transverse magnetic (TM) mode data uses strike-parallel magnetic fields and strike-perpendicular electric fields. The apparent resistivity and phase curves are shown for four representative MT stations across central Taiwan and display the high-quality of these measurements. Data curves shown adjacent the Lishan Fault reveal a discontinuous change in the TM mode response across this feature, with low resistivity at long-period to the west and high resistivity to the east. The discontinuous behaviour could be due to vertical current channeling as excess near surface currents generated in the Philippine Sea dissipates downwards into the mantle beneath Taiwan. A sub-vertical conductive fault, such as the LF, would provide a conductive window facilitating the dissipation of electric current to depth and cause abrupt changes in the

slope and phase of the TM mode response (Park et al., 1991). The near surface resistivity (short periods) can be seen to increase across Taiwan from west to east and is associated with the increase in metamorphic grade. Station TGR295 was installed in the Longitudinal Valley and shows relatively low near surface resistivity as expected for recent sediments in this area.

The vertical magnetic fields data are displayed in the lower panels of Figure DR3 as in-phase (real) and out-of-phase (imaginary) components of tipper. Tipper data represent ratios of the vertical to horizontal magnetic fields. Decreasing values of the real component reflect the influence of the conductive Philippine Sea. The skin-depth phenomenon governs the sensitivity of MT periods at depth; longer period signals sample greater volumes of the earth. Thus, for station TGR235 in western Taiwan, the decrease to negative in-phase tipper values occurs at a period T = 2000s; in central Taiwan near the Lishan Fault negative values occur for periods T > 1000s. On the east coast, all in-phase tipper data are negative (TGR295), reflecting the close proximity to the Philippine Sea.

Smooth curves in Figure DR3 indicate the fit to the measured MT data for the inversion model in Figure 2. At all stations, an acceptable fit to the measured MT data was obtained.

3. Inversion Modeling of the MT Data

The 2-D regularized MT inversion algorithm of Rodi and Mackie (2001) was used to generate resistivity models from these MT data. Error floors of 20%, 7.5% and 0.03 were used for the apparent resistivity, phase and tipper data, respectively. Setting a lower error floor for the phase than for the apparent resistivity downweights the apparent resistivity data and reduces the influence of static shifts. To additionally address the static shifts, the inversion model included topography, and the algorithm was set to solve for the static shift coefficients at each site during late stage iterations. Regularization (smoothing) parameters were set to $\tau = 3$ (trade-off parameter that balances data fit against model smoothness) and $\alpha = 3$ (ratio of horizontal to vertical smoothing). This choice of parameters was found to balance the competing requirements to generate a spatially

smooth model and produce a low data misfit.

3.1 Pseudosections

Figure DR4 displays pseudosections of the data and inversion model response for a) the TM mode, b) the TE mode and c) the tipper data. All stations plotted in these pseudosections show good agreement between measured MT data and the predicted model response. White regions in the pseudosections indicate data that were excluded from 2-D inversion modeling because of high levels of noise and/or severe distortion. The increase in resistivity eastwards across Taiwan, observed in the sample data curves (Figure DR3), is also clearly visible in the TE and TM mode pseudosections. Further, the effect of the Philippine Sea, which decreases the in-phase tipper data, is observed at progressively shorter periods eastwards across Taiwan.

3.2 Constrained Inversions

MT data are sensitive to the conductance (integrated conductivity) of a layer. A plot of conductance versus distance for the fixed inversion models helps to illustrate how the inversion algorithm is able/unable to fit the data subject to the imposed constraints. Figure DR5 illustrates that for the F20 and F30 models, the integrated conductance to a depth of 60km beneath the profile is similar to that achieved in the unconstrained (free) inversion model, where no constraint was imposed on the basement depth. In contrast, with a resistive basement fixed at 10km, the inversion model shows oscillatory behaviour beneath the LF, very different than the other model responses. This behaviour illustrates how the F10 inversion is forced to over-emphasize shallow (<10km) features of alternating high–low conductivity in order to fit the data.

To illustrate that the inability of the inversion algorithm to fit the measured MT data with the F10 model is robust, the same fixed inversion models as used in our manuscript have been generated with regularization values of α=1 and τ=1. These regularization values will minimize the smoothing constraint compared to the choice of α=3 and τ=3. Generating the same conductance versus distance plot for these rougher inversion models

indicates the inversion algorithm is still unable to fit the F10 model (Figure DR6). This test indicates a resistive basement fixed at 10km is not compatible with the data near the LF, regardless of regularization constraint.

4. Archie's Law Calculations

A range of pore fluid salinity which best represents the PT conditions expected in the mid to lower crust of central Taiwan was used in the manuscript to estimate porosity from Archie's equation. However, it is important to note that the interpretation does not depend upon the specific value of porosity. Rather, the key point is that the resistivity of the LFC can be explained by small (realistic) porosity values. These interconnected saline fluids, will lower electrical resistivity more than seismic velocity, giving rise to the distinct LFC domain observed in the v_p - ρ crossplot.

The pore fluid resistivity values used in the porosity calculations were in the range ρ_w = 0.01 – 0.05 Ωm and were the same as those used by Wannamaker et al. (2002) for investigation of a similar conductive feature in the mid to lower crust of the South Island, New Zealand. This range of resistivity values corresponds to pore fluid salinities in the range 4 - 25% by weight and with pressure > 3kbar and temperatures > 250°C (Nesbitt, 1993). Salinities exceeding 20% by weight have been observed in lower crustal fluid inclusions (Shmulovich and Graham, 1996; Aranovich and Newton, 1996).

Despite an attempt to choose representative values, the calculation of a few percent porosity is not highly sensitive to the range of pore fluid salinity chosen. For example, if the estimated salinity was 100% greater (ie. assume an upper limit of ρ_w = 0.1 Ωm), then this value would yield a porosity of 3.5%, which is still consistent with our interpretation.

Further, the cementation exponent m, which is an empirical parameter describing the degree of pore connectivity does not have a significant influence on our interpretation. Values for m typically vary between limits of 1 (high pore connectivity) and 2 (low pore connectivity). Calculations in our manuscript defined m = 1.5 resulting in the porosity estimations of 1-2%. At the extremes, assuming m = 1 would yield a porosity range of 0.07% – 0.3%, and m = 2 would give a porosity range of 2.6% – 5.8%.

Figure DR7 shows the variation of porosity with values of pore fluid salinity and cementation exponent required to explain a bulk resistivity value of 15 Ωm.

5. References

Aranovich and Newton, Contributions to Mineralogy and Petrology, 125, 200-212,1996).

Nesbitt, B., 1993, Electrical resistivities of crustal fluids: Journal of Geophysical Research, v. 98, p. 4301-4310.

Park, S.T., Biasi, G.P., Mackie, R.L., and Madden, T.R., 1991, Magnetotelluric evidence for crustal suture zones bounding the southern great valley, California: Journal of Geophysical Research, v. 96, p. 353-376.

Rodi, W., and Mackie, R.L., 2001, Nonlinear conjugate gradients algorithm for 2-D magnetotelluric inversion: Geophysics, v. 66, p. 174-187.

Shmulovich and Graham, Contributions to Mineralogy and Petrology, 124, 370-382, 1996;

Wannamaker, P.E., Jiracek, G.R., Stodt, J.A., Caldwell, T.G., Gonzalez, V.M., McKnight, J.D., and Porter, A.D., 2002, Fluid generation and pathways beneath an active compressional orogen, the New Zealand Southern Alps, inferred from magnetotelluric data: Journal of Geophysical Research, v. 107, doi:10.1029/2001JB000186.

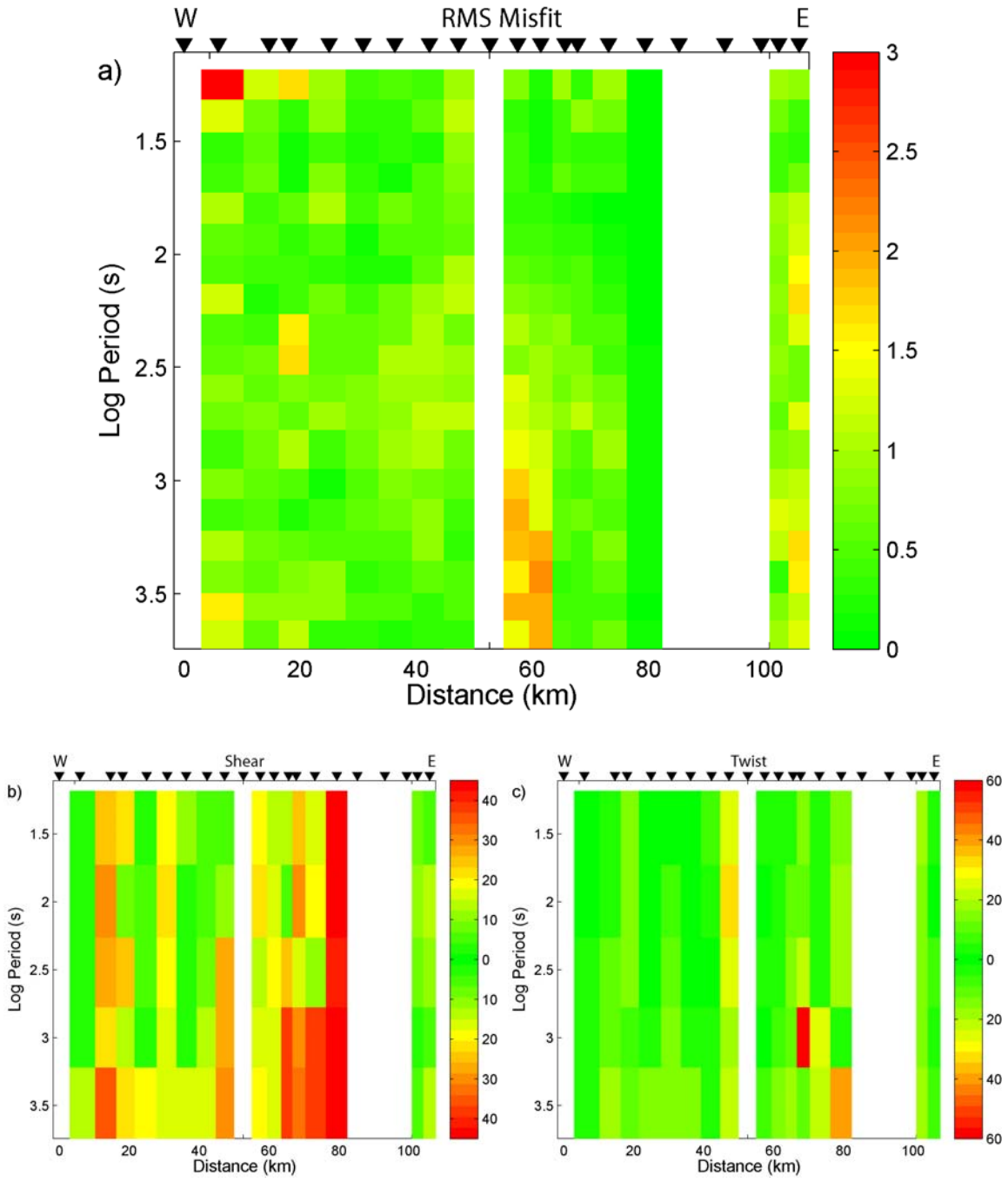

Fig DR1. **a)** Root-mean-square (RMS) misfit from tensor decomposition of long-period MT data recorded in central Taiwan. The low misfit values (< 1.5) at most stations and periods indicate that the 2-D strike direction obtained is well constrained. **b)** Shear and **c)** Twist distortion parameters from tensor decomposition. Higher values of the twist and shear angles indicate greater distortion of the MT data. While values of the shear angles are higher than the twist angles, these parameters indicate minor galvanic distortion, especially for periods sensitive to the upper and mid crust. White bands indicate where electric field data was excluded from 2-D analysis due to strong distortion (see Fig. DR4).

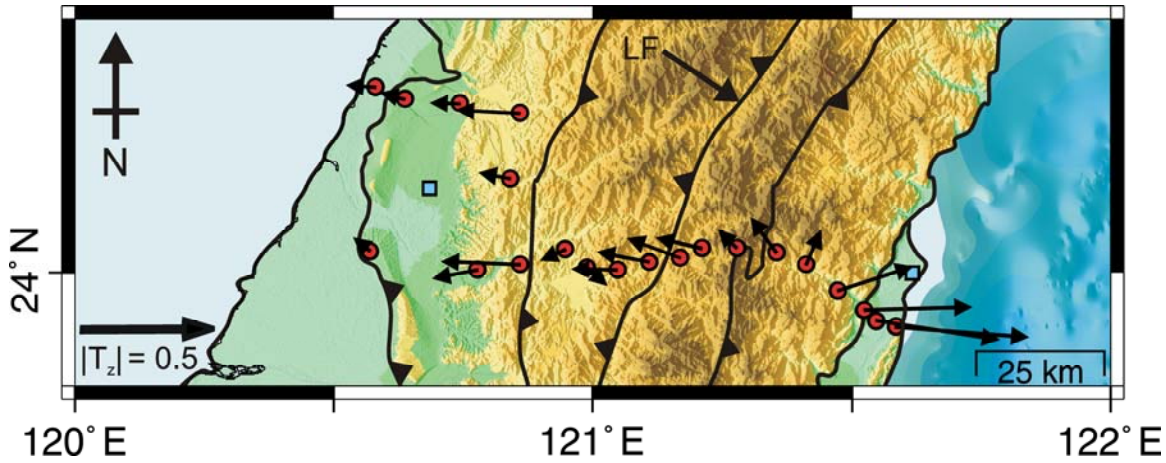

Fig DR2. Induction vectors (Parkinson convention) averaged over the periods range 10 – 100s. These vectors are predominately perpendicular to the geological boundaries, indicating 2-Dimensional resistivity structure within the upper and mid crust. Some scatter is observed, especially in eastern Taiwan near the Philippine Sea. However, the strike-perpendicular (2-D) behaviour of these vectors adjacent the Lishan Fault (LF) in central Taiwan indicates a relatively 2D structure.

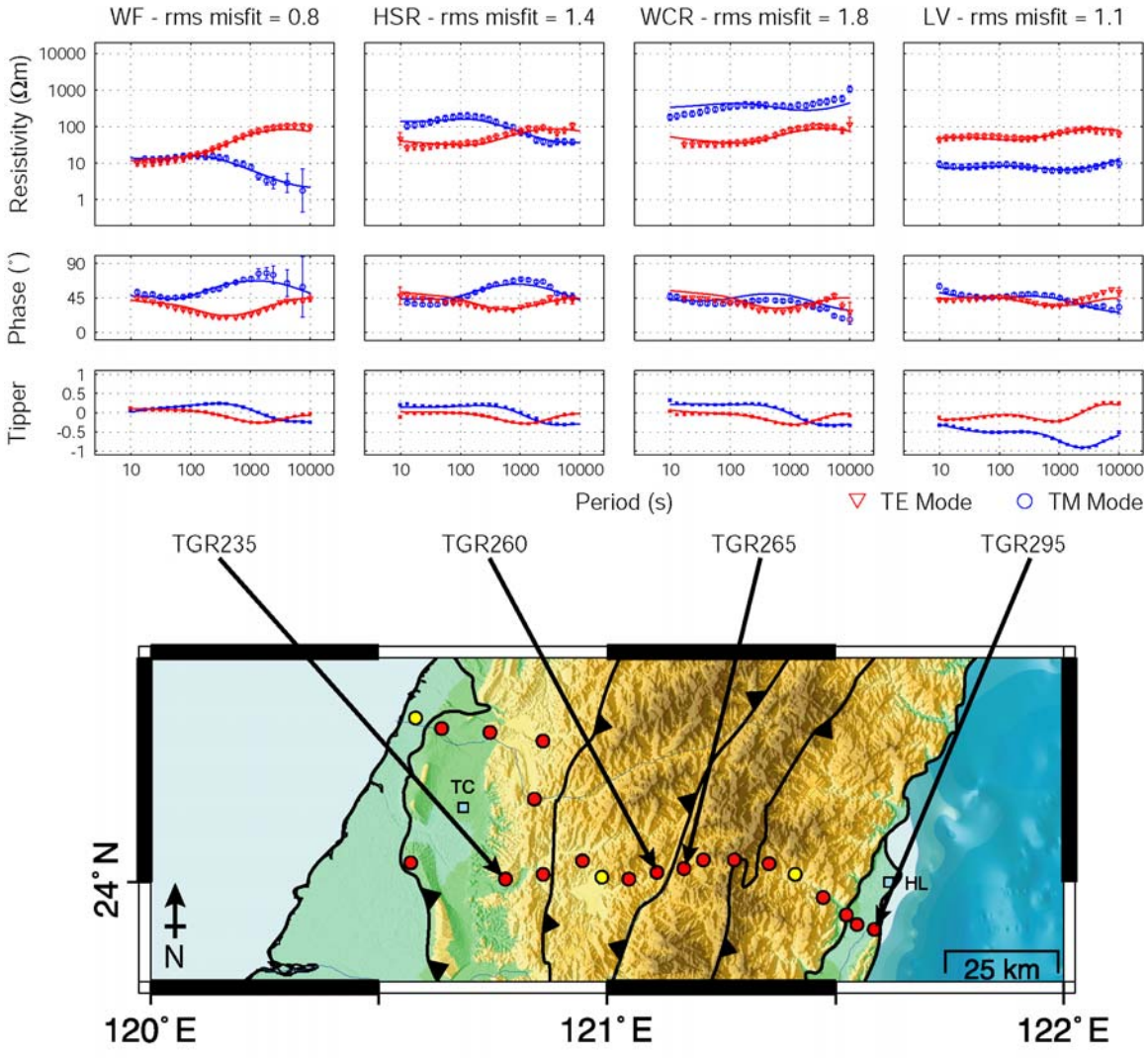

Fig DR3. Sample long-period MT data curves from central Taiwan. Geological provinces and boundaries are identified on the inset map: Western Foothills WF, Hseuhshan Range HSR, West Central Range WCR, and Longitudinal Valley LV. Red circles denote locations of long-period MT data and yellow circles indicate where only magnetic fields data were analyzed. Major cities in central Taiwan are: Taichung TC and Hualien HL. Smooth MT curves show the fit to the observed MT data for the model in Figure 2. In the tipper plots, in-phase (real) and out-of-phase (imaginary) data and responses are indicated by blue and red colours, respectively. Data curves displayed in the two middle panels (TGR260 and TGR265) are adjacent the Lishan Fault and a significant change in the TM mode at long-period can be observed across this feature.

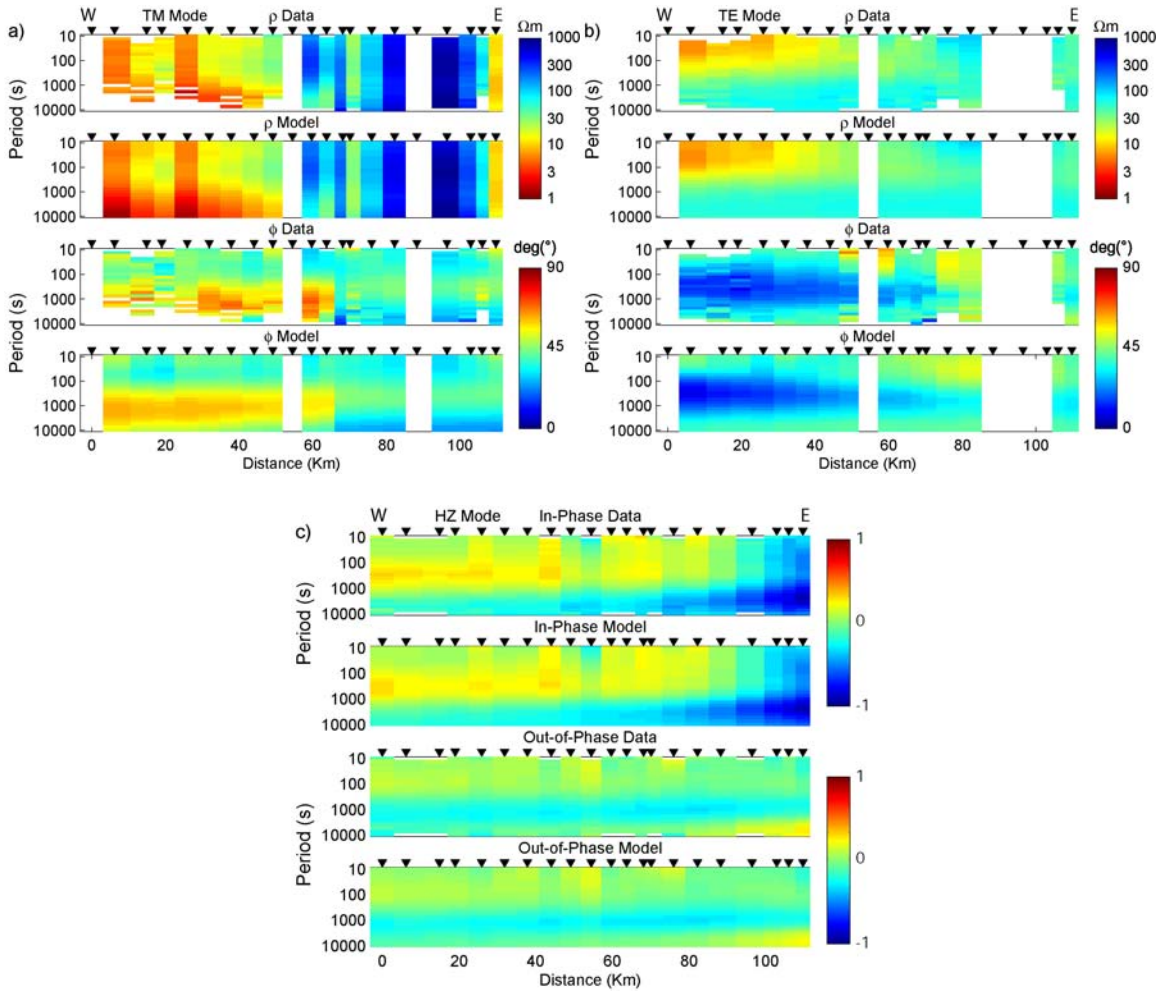

Fig DR4. Pseudosections of long period MT data collected in central Taiwan. The measured and modeled resistivity and phase data are displayed for **a)** the TM (transverse magnetic) mode polarization and **b)** the TE (transverse electric) mode polarization. **c)** Measured and modeled in-phase (real) and out-of-phase (imaginary) tipper data are displayed. White regions in the pseudosections indicate data that were excluded from 2-D inversion modeling because of high levels of noise and/or severe distortion.

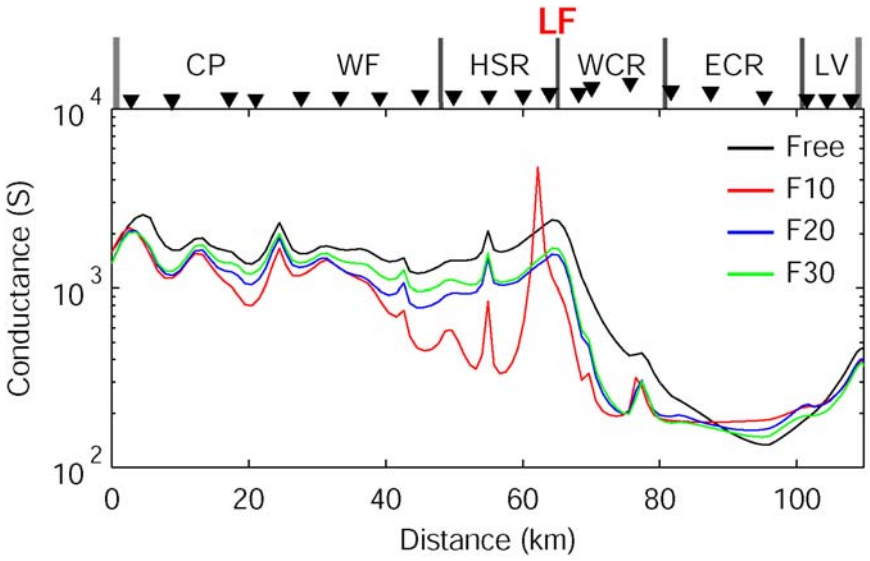

Fig DR5. Conductance along profile for α=3, τ=3 TETMHZ inversion models.

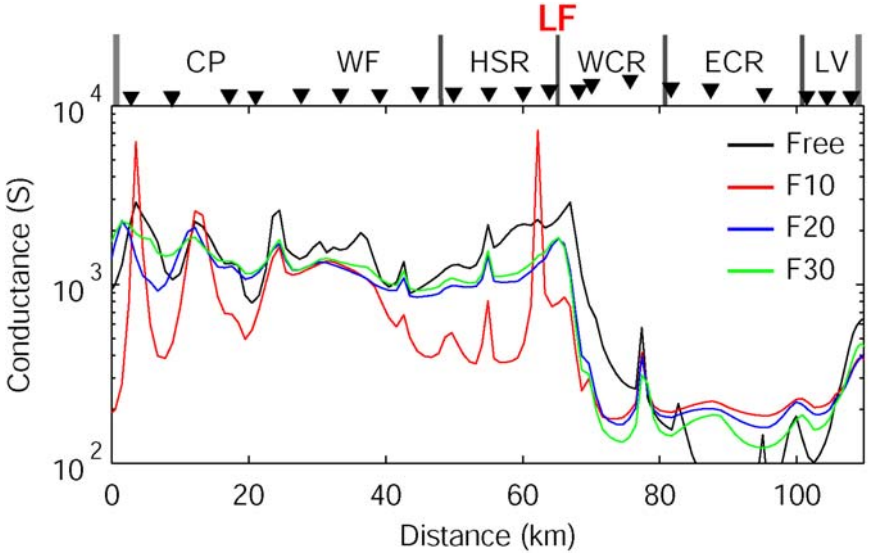

Fig DR6. Conductance along profile for α=1, τ=1 TETMHZ inversion models.

The overall RMS misfits for the TETMHZ inversion models are:

	F10	**F20**	**F30**	**Free**
α = 1, τ = 1	1.98029	1.79360	1.66410	1.13116
α = 3, τ = 3	2.11384	1.86826	1.77038	1.30355

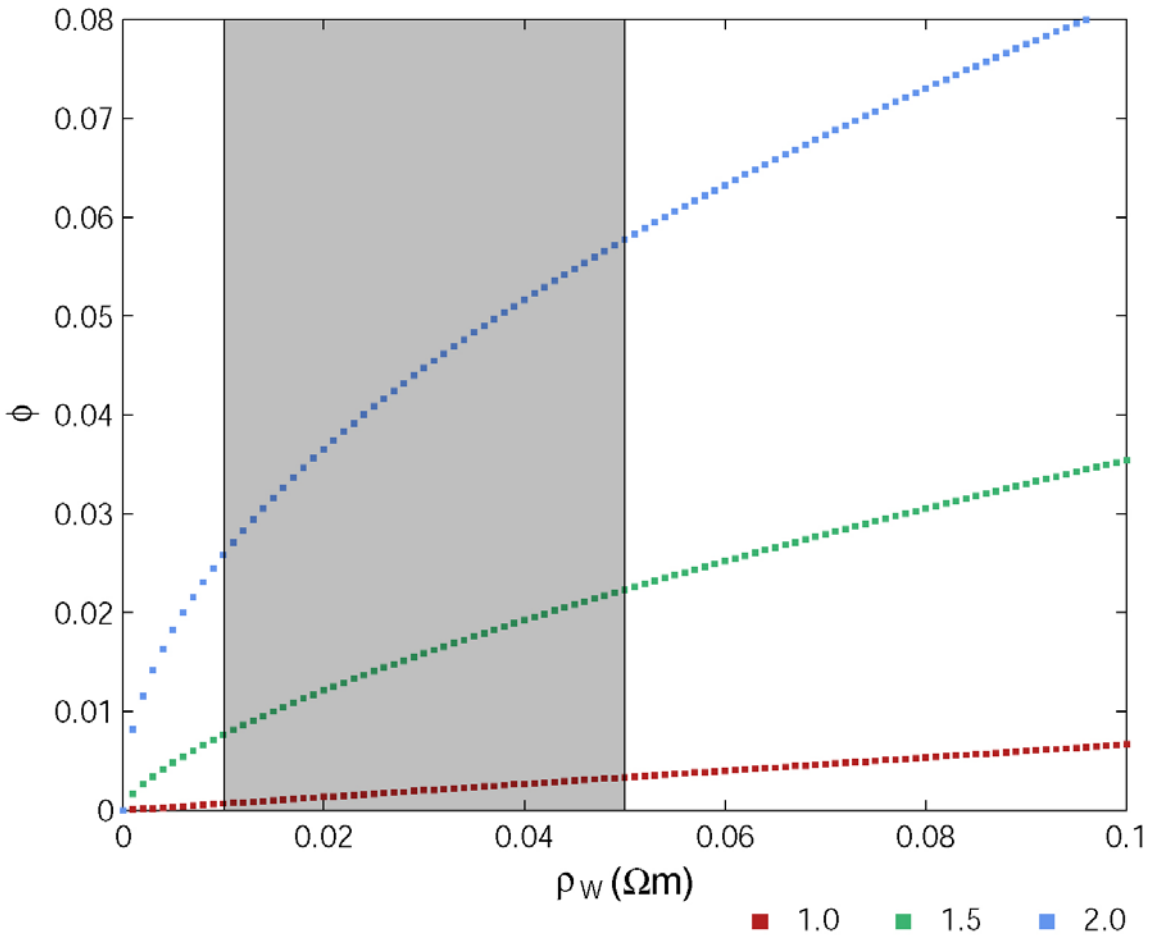

Fig DR7. Archie's law porosity estimates. Legend indicates the value of cementation exponent (m) used in the calculations. Shaded region denotes the range of pore fluid resistivity (ρ_w) used in the manuscript. Calculations assume a bulk resistivity of 15 Ωm.